Journal of
Engineering Sciences
Faculty of Engineering
Assiut University
JES
مجلة
العلوم الهندسية
كلية الهندسة
جامعة أسيوط
journal homepage: http://jesaun.journals.ekb.eg

Response analysis of hollow core Slab Bridge with different column heights to near-fault seismic motions

Received 5 April 2025; Revised 5 July 2025; Accepted 6 July 2025

Sayed Mahmoud[1]
Ahmed A. Soliman[2]
Magdy M.M. Genidi[3]
Waleed Abdallah[4]

Keywords
Near-Fault; Fling-step; Forward-directivity; frequency content, hollow core slab bridge.

Abstract: The near-fault earthquake motions are characterized by influential velocity impulses, and remarkable permanent displacement. Such unique characteristics can substantially change the induced seismic responses of structures. The current study incorporates near-fault earthquake motions with forward-directivity and fling-step to excite a reinforced concrete (RC) hollow-core slab bridge with varying column heights. The study adopts a RC hollow-core slab bridge having three spans, each 30.0 m long, with a deck width of 11.5 m, a depth of 2.0 m and column's heights designed to meet a span-to-column height ratio of 2.5 to 5. Three-dimensional numerical models of the bridge are established using the CSI-BRIDGE software and dynamic time-history analysis is used to capture the simultaneous influence of near-fault motions and supporting columns with varying heights on the seismic response of the RC hollow-core slab bridge, under selected earthquake loads. Upon analyzing the seismic response of the excited bridge, the simulation results revealed that a substantial increase in seismic demands of the bridge with more susceptibility to near-fault motions with fling-step than the forward directivity ground motions. This effect is more pronounced for bridge models with taller columns than models with reduced column's height.

1. Introduction

Near-fault earthquake motions are considered harmful type of ground motions due to the contained numerous crucial characteristics such as generated velocity pulses, and permanent displacement. Near-fault records contain two types of velocity pulses according to the mechanism of the fault-rupture. The one with two-sided pulses is called forward-directivity. On the other hand, the one with Permanent displacement denotes the enduring deformation of the Earth's surface induced by the ground motions. Records characterized as near-fault earthquakes with forward-directivity and fling-step may cause considerable damage to the excited structures.

[1] Professor, Civil and Construction Engineering Dept., Imam Abdulrahman Bin Faisal University, Saudi Arabia. elseedy@hotmail.com & smabdein@iau.edu.sa
[2] PHd. Candidate, Civil. Engineering Dept., Helwan University, Mataria, Egypt, civil.ahss@gmail.com
[3] Assoc. Professor, Civil. Engineering Dept., Helwan University, Mataria, Egypt , magdygenidi0@gmail.com
[4] Assoc. Professor, Civil. Engineering Dept., Helwan University, Mataria, Egypt , waleed_abdallah@m-eng.helwan.edu.eg.com

https://doi.org/10.21608/jesaun.2025.373003.1471

Held structures in the near-fault vicinity are at risk from damage point of view due to the combined effects of the features of the near-fault earthquake motions that pose potential seismic hazards leading to significant seismic damages [2]. Findings from the performed studies clearly indicated that the captured seismic response and collapse mechanism were significantly influenced by the frequency content of excitation records and existence of pulses [3-5]. The impact of velocity pulses on the seismic response of various types of structures has been studied demonstrating that the captured structural damage can be due to the existence of velocity pulses which place significant demands on structures [6-8]. Seismic performance of concrete gravity dams to near-fault and far-fault earthquakes has been studied employing dynamic time-history analysis considering assessment of damage levels [9]. Park et al. [10] utilized the near-fault earthquake records from 1999 Düzce to examine its impact on the Bolu Viaduct. Large deformations due to the existence of velocity pulses have been captured. Several studies have been conducted to evaluate the vulnerability of structures subjected to near-fault records, revealing a substantial increase in displacement demands [11-14].

Due to the severity of damage of structures located in the near-fault region, construction of bridges in these regions is always avoided. However, due to the necessity of bridges in local and national transportation networks, and supporting economic development worldwide, they are needed to link main routes and connecting remote areas which may require constructing some bridges close to faults [15]. Consequently, evaluating the performance of bridges under near-fault motions is crucial to ensure their functionality, and life safety. Seismic responses of bridge structures subjected to near-fault records with velocity pulses and the relatively large spatial permanent displacements have been studied showing different catastrophic mechanisms through the reported numerical simulations [16-18]. Several fault-crossing bridges have been numerically and experimentally investigated revealing sustained damage during significant seismic records including 1995 Kobe, 1999 Chi-Chi, and 1999 Duzce [19]. Historical events, such as the 1999 Kocaeli, earthquake, have demonstrated that structures exposed to near-fault ground motions often sustain more severe damage than expected [20]. The Performance of continuous rigid-frame bridges subjected to near-fault motions has been investigated showing substantial increase in the induced response to pulse-like records compared to non-pulse-like ones [21]. Zheng et al. [22], conducted a study to investigate the simultaneous effect of velocity pulses and soil-structure interaction on the seismic response of long-span, asymmetrical suspension bridges. Seismic response analysis of a long-span concrete-filled steel tubular arch bridge has been examined three different types of ground motions including records with fling-step to deeply understand the influence of records with fling-step [23].

performance-based seismic assessment of buildings has been carried out employing the simultaneous effect of dynamic characteristics of excitation records and building height of multi-story RC frame buildings in Australia using numerical modelling and time-history analysis. Fragility analysis was then conducted for the considered buildings under all the selected ground motion records [24, 25]. Srivastava et. Al., [26] used the fragility analysis to investigate the effect of material and geometric properties on the seismic response of bridges accounting for a wide range of pier height-to-width ratios. short or moderately tall bridges or bridges with extremely slender columns have been considered in the analysis. The effect the

vertical component of earthquake records on the seismic behaviour of typical continuous RC bridges has also been investigated [27]. Sequential earthquakes from near-fault regions were also used to excite girder bridges to assess the seismic damage using Nonlinear time-history analysis [28]. The novelty of the current research study lies in its focused investigation of the seismic behavior of RC hollow core slab bridges subjected to near-fault earthquake motions, specifically those exhibiting forward-directivity and fling-step effects. While near-fault seismic impacts have been examined in previous studies, the behavior of hollow core slab bridges under these specific ground motion characteristics remains largely unexplored. The study conducts detailed numerical simulations using CSI-BRIDGE on a realistic three-span bridge model, incorporating parametric variations in column height to evaluate their effect on the induced seismic response. By quantitatively evaluating the effects of forward-directivity and fling-step on structural performance, this study provides new insights into the vulnerability and design considerations for hollow core slab bridges located in proximity to active fault regions offering a meaningful contribution to bridge design applications and academic literature as well.

2. Bridge Modelling

2.1. Bridge configuration

Fig. 1 presents the longitudinal-sections of the considered bridge models for hollow-core bridges considered in the current study. The bridge has been designed following the requirements of the Egyptian Code for RC bridges [29]. The main structural components of the bridge include the deck, supporting columns, and abutments. The bridge has three spans; each span is 30.0 m long together with a deck of 11.5 m wide and 2.0 m deep. The bridge considered herein is supported by portal frame piers and abutments, with designed dimensions and detailed reinforcement specifications provided in Figs. 2 and 3. Elastomeric pads linked to the abutments are used to support the superstructure of the bridge which is monolithically connected to the piers. The supporting piers have a rectangular RC cap of 1.0 m width and 6.0 m length. Detailed dimensions and reinforcement details for a typical pier are shown in Fig 2.

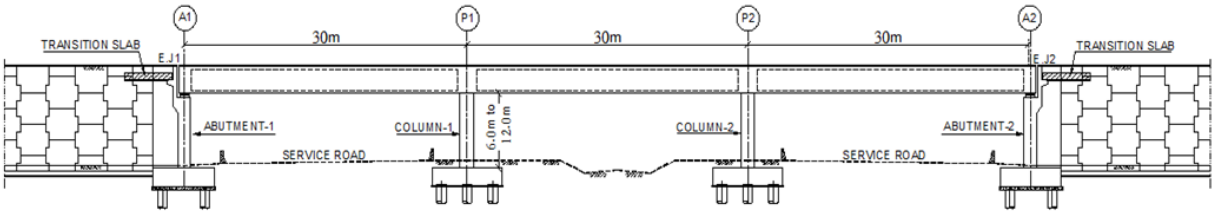

Figure 1. Longitudinal-section of the considered bridge models for hollow-core bridge

The designed bar diameters for both transverse and longitudinal reinforcements are 12 mm and 32 mm, respectively. The designed reinforcement ratio of the pier-column longitudinal reinforcement is 2.26%. The calculated volumetric reinforcement ratio of the spirals is 0.8%. The reinforcement details and values of the pier are provided in Fig. 2. 11 Φ 32 bars are used

to reinforce the pier around the curved section and 28 Φ 32 bars are distributed around the straight portion. Φ 12@100 mm is used as a transverse spiral reinforcement at both the start and end of the pier, while Φ 12@125 mm is distributed along the middle of the pier. The designed reinforcement for the abutment is provided in Fig. 3. Deep foundations of bearing piles of designed 1.0 m diameter are used to support both abutments and piers.

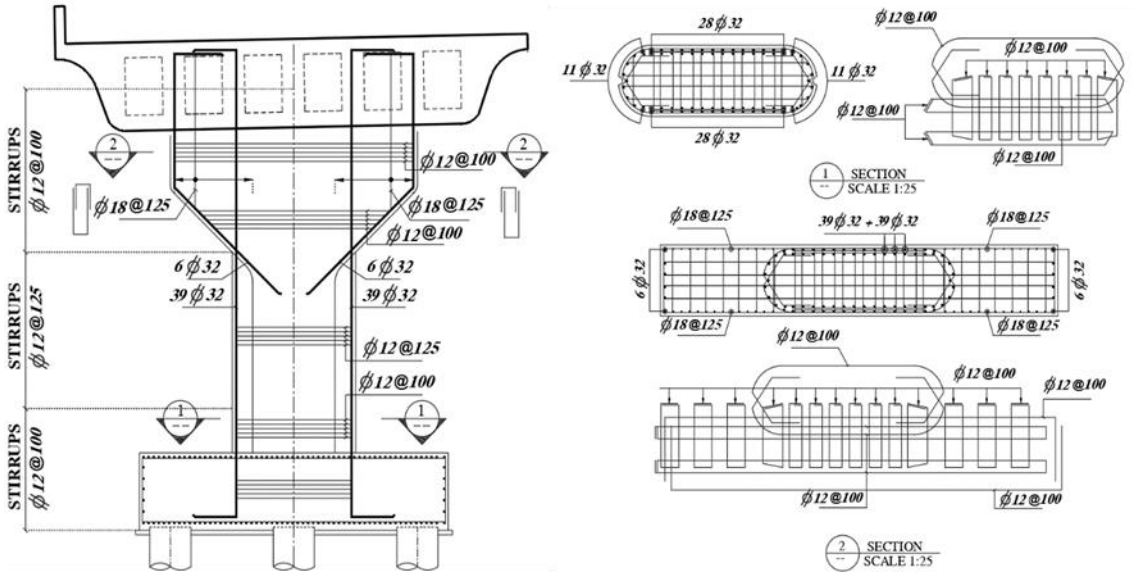

Figure 2. Reinforcement details of a supporting column in longitudinal and transverse directions.

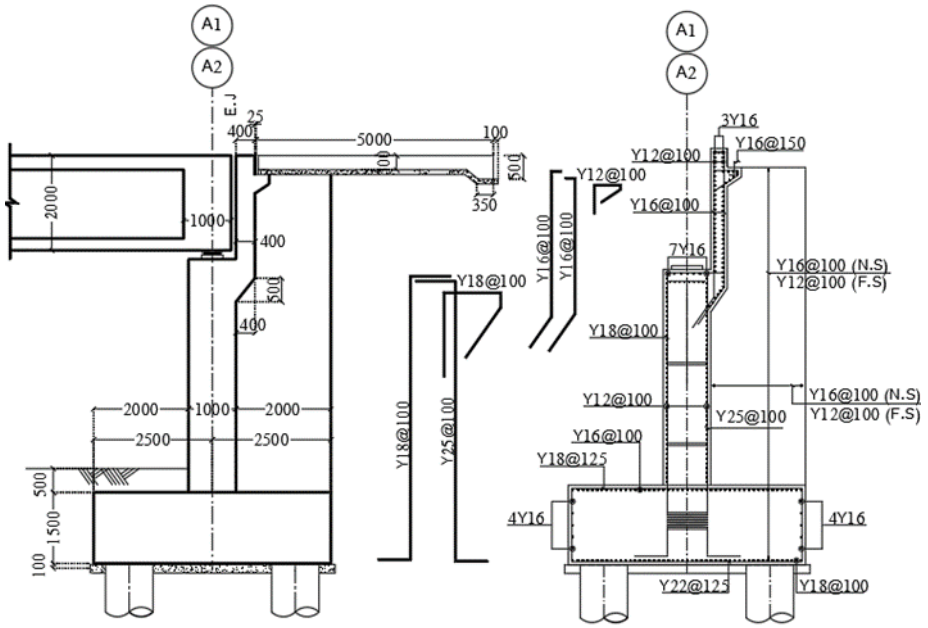

Figure 3. Reinforcement details of the abutment in longitudinal and transverse directions.

The boundary conditions at the base were represented with extra care utilizing shell finite element objects, with pile caps of the abutments and columns considering thicknesses of 1.50 m and 1.75 m, respectively. This has been performed to properly represent the interaction between the supporting ground and the bridge. Soil-structure interaction (SSI) was considered by introducing spring elements in longitudinal, transverse, and vertical directions with

stiffness values calculated based on subgrade reaction modulus determined from geotechnical field investigations on the bridge site of Damanhur City. The clayey silts and sandy clay layers in the soil profile with varying stiffness were represented by general site conditions. Both the 2700 kN capacity piles and 20m depth piles are expected to settle approximately 10 mm. As an end-bearing pile, both have a vertical stiffness of 270,000 kN/m and lateral stiffness of 30,000 kN/m.

2.2. Developed bridge models

Fig. 4 presents the developed finite element models of the analyzed bridges in the current study. Five bridge models were developed using the CSI-BRIDGE software. Three elastomeric bearings were used to allow the lateral movement at the edge abutments. The modelled intermediate columns are monolithically connected to the deck to provide the needed fixation joints. The developed models have varying columns of heights from 12.0 m to 7.5 m. The selected columns heights have a satisfy span-to-column height ratio of 2.5 to 5. The developed models were excited using the selected near-fault records. The grillage method was utilized to model the bridge deck, in which it is idealized as a network of interconnected beam elements or grillages, with constraints applied at their joints. The main beams are represented by the arrangement of longitudinal grillage members. The transverse arrangement of grillage members represents the deck slab and diaphragm beams. The required longitudinal and transverse stiffness for the continuous deck is gained through the arrangement of longitudinal and transverse beam elements assuming linear elastic behavior. The section properties for the grillage element are calculated first then assigned to beam-column elements, which is modelled as linear elastic using nonlinear three-dimensional beam-column elements, with tributary mass lumped at each node of the grillage system. As shown in Fig. 4, the bridge deck is divided into segments with their local axes. The connection between the deck and supporting abutment is modelled as an integral connection without bearings. In the developed bridge model, the abutment is modelled using a rigid element of the same length as the superstructure’s width. To accommodate the arising lateral and vertical displacements, elastomeric bearings at the expansion joint locations are utilized in the developed model. The behavior of the developed elastomeric bearings is controlled by their shear deformation capacity.

2.3. Design loads

Regarding the design loads, a wide variety of loads have been taken into account during the analysis and design process. These loads include permanent loads in terms of dead and superimposed dead loads which act on the bridge throughout its life. Transient loads, which act for a short period such as live load, is one of the considered design loads. In addition, hypothetical design vehicles based on truck loading or equivalent lane loading were considered in the design as well. Seismic forces that often control bridges design particularly in regions with high level of seismicity were also considered consideration.

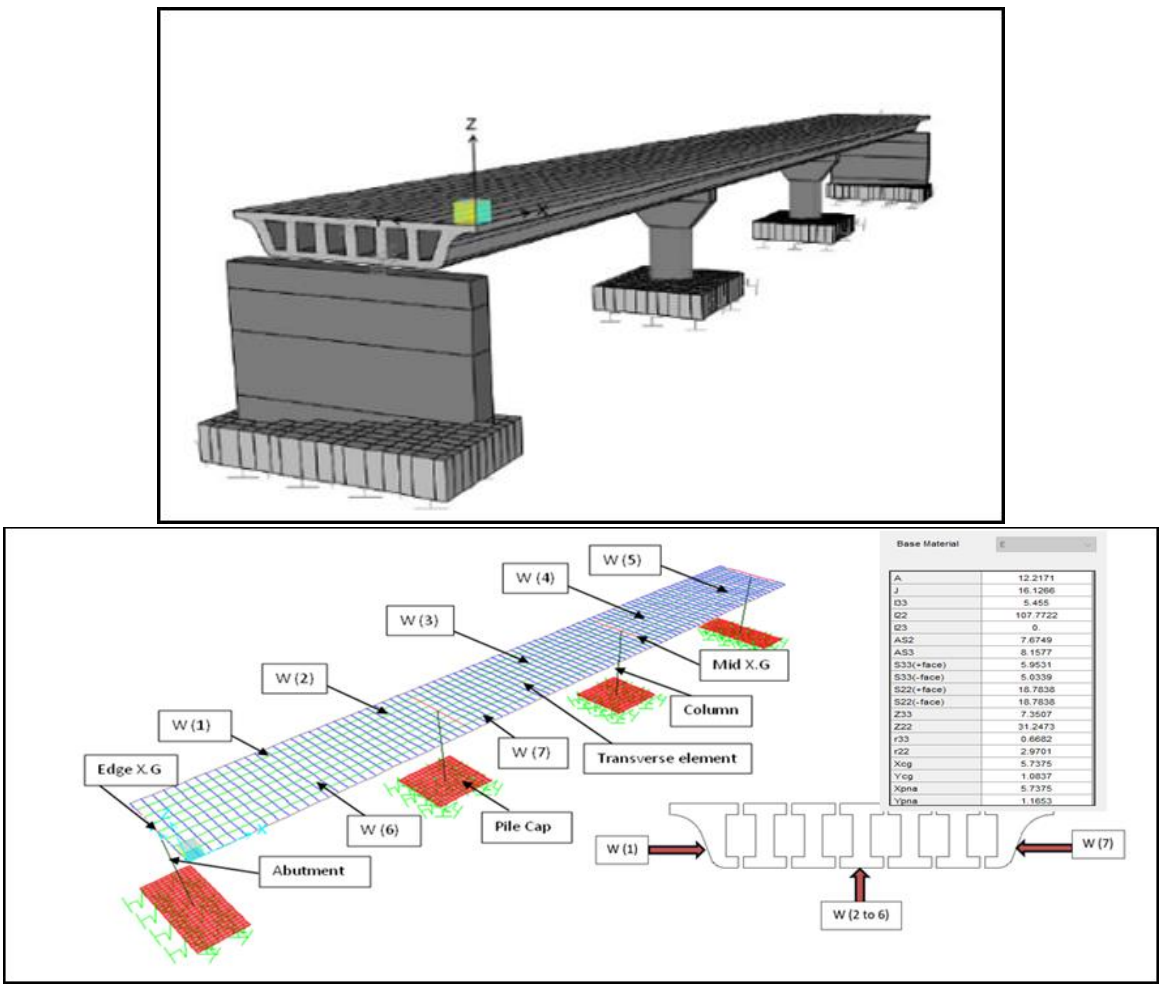

Figure 4. Developed hollow-core deck slab bridge model.

3. Material Properties

3.1. Concrete and steel properties

RC is one of the most commonly used construction materials all over the world. RC provides a unique coupling of concrete and steel as composite materials of entirely different mechanical properties. For accurate modelling of concrete behavior during the simulation analysis, the utilized herein CSI-Bridge software requires the constituent materials' properties as well as the linear and multilinear isotropic properties. The assigned characteristic compressive strength of concrete for superstructure and substructure elements is 40 MPa, (i.e., $f_{cu} = 40\ MPa$) and the corresponding modulus of elasticity $E_c = 27828\ MPa$. The input value for tensile concrete strength is almost 3.4 MPa, (i.e., $f_{ct} = 3.8\ MPa$) and Poisson's ratio of 0.2. The assigned yield strength for main steel reinforcement is 40 MPa, (i.e., $f_y = 360\ MPa$). The same yield strength value has been assigned to the transverse reinforcement bars. An elastic modulus for steel reinforcement of 200000 MPa, (i.e., $E_s = 200000\ MPa$) was used for performing the analysis. The aforementioned material properties were determined from the construction blueprints. The CSI-Bridge software utilized efficiently models the behavior of both concrete and steel materials based on the input properties.

3.2. Elastomeric bearings

The used elastomeric bearings at the piers and abutments, which allow the longitudinal movement of the supported superstructure, are modelled using a link element with predefined stiffness properties. The movement of the elastomeric bearings is controlled by the limits of the elastomer's flexibility, and the behaviour is governed by shear deformations capacity of the bearings. The presented Fig. 7 shows the idealized force-displacement relationship of the isolation system. k1 refers to the stage of elastic stiffness, k2 defines the stage of post-elastic stiffness, and Q identifies the characteristic strength. dy and Fy respectively denote yield displacement and the corresponding yield force of the isolator. The induced peak force and peak displacement by the isolator are identified as fmax and dmax. The time period of the isolation system, T, following the formula provided in Eq. (1) as:

$$T = 2\pi\sqrt{\frac{W}{k_2 g}} \tag{1}$$

Where, W, is the weight supported by the isolator, and g, is the acceleration of gravity.

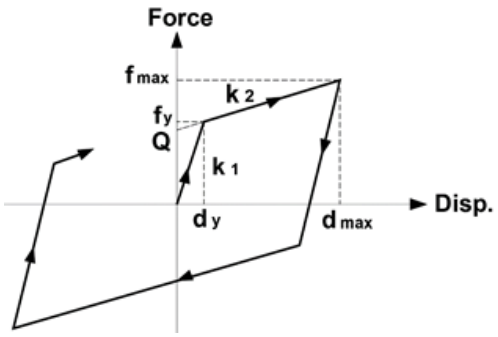

Figure 5. Idealized force-deformation relationship of the isolation system.

4. Ground motion dataset

The study utilized 14 near-fault ground motions; half of the records represent forward-directivity category, and the other half represent fling-step records. The main difference between the two sets is the existence of a two-side pulse in the velocity time-history of the forward-directivity category and a one-sided pulse in the velocity time-history of fling-step category. The formation of one-sided pulse causes a permanent displacement in the ground. The selected records to represent the forward-directivity are listed in Table 1 and those records to represent fling-step are listed in Table 2. The records name, station, magnitude, time duration, peak ground acceleration (PGA), peak ground velocity (PGV), and the ratio PGA/PGV are all provided in the Tables. The calculated ratios of PGA/PGV clarify that almost all selected are of low-frequency content [30] see also Figs 6 and 7. The selected sets of records are scaled to fit Cairo region, (i.e., PGA of 0.125g). the plotted response spectra for each individual set of records are presented in Figs 8. Both sets of records are selected from the Pacific Earthquake Engineering Research Center (PEER). Similar earthquake records have been used to investigate the performance of RC buildings and structures with different slab systems [31, 32].

Table 1: Near-fault ground-motion records input with forward directivity.

Earthquake (record)	Station	PGA (g)	PGV (cm/sec)	PGD (cm)	PGA/ PGV	M_w	t_d (s)
Cape-Mendocino	Petrolia-90	0.66	88.5	33.2	0.75	7.0	25
Erzincan-EW	Pacoima Dam 279	0.50	78.12	28.02	0.64	6.7	20
Tabas	Ferdows	0.87	123.3	93.57	0.71	7.3	32
Loma-Prieta	LGPC-00	0.57	96.05	41.92	0.59	6.9	25
Loma-Prieta	Lexdam-00	0.41	95.73	30.27	0.43	6.9	15
Northridge	Rinaldi-275	0.87	147.92	41.86	0.59	6.7	15
Northridge	Oliveview-360	0.84	129.31	32.11	0.65	6.7	15

PGA, peak ground acceleration; PGV, peak ground velocity; PGD, peak ground displacement; M_w, magnitude; t_d, time duration.

Table 2: Near-fault ground-motion records input with fling-step.

Earthquake (record)	Station	PGA (g)	PGV (cm/sec)	PGD (cm)	PGA/ PGV	M_w	t_d (s)
Chi-Chi NS	TCU-052	0.45	172.24	226.5	0.26	7.6	90
Chi-Chi EW	TCU-052	0.36	151.13	210.3	0.24	7.6	90
Chi-Chi EW	TCU-065	0.79	125.28	108.7	0.63	7.6	90
Chi-Chi EW	TCU-068	0.51	248.50	297.0	0.21	7.6	90
Chi-Chi NS	TCU-068	0.37	263.96	421.0	0.14	7.6	90
Chi-Chi EW	TCU-074	0.59	70.33	21.31	0.84	7.6	90
Chi-Chi NS	TCU-084	0.43	48.07	20.44	0.89	7.6	90

PGA, peak ground acceleration; PGV, peak ground velocity; PGD, peak ground displacement; M_w, magnitude; t_d, time duration.

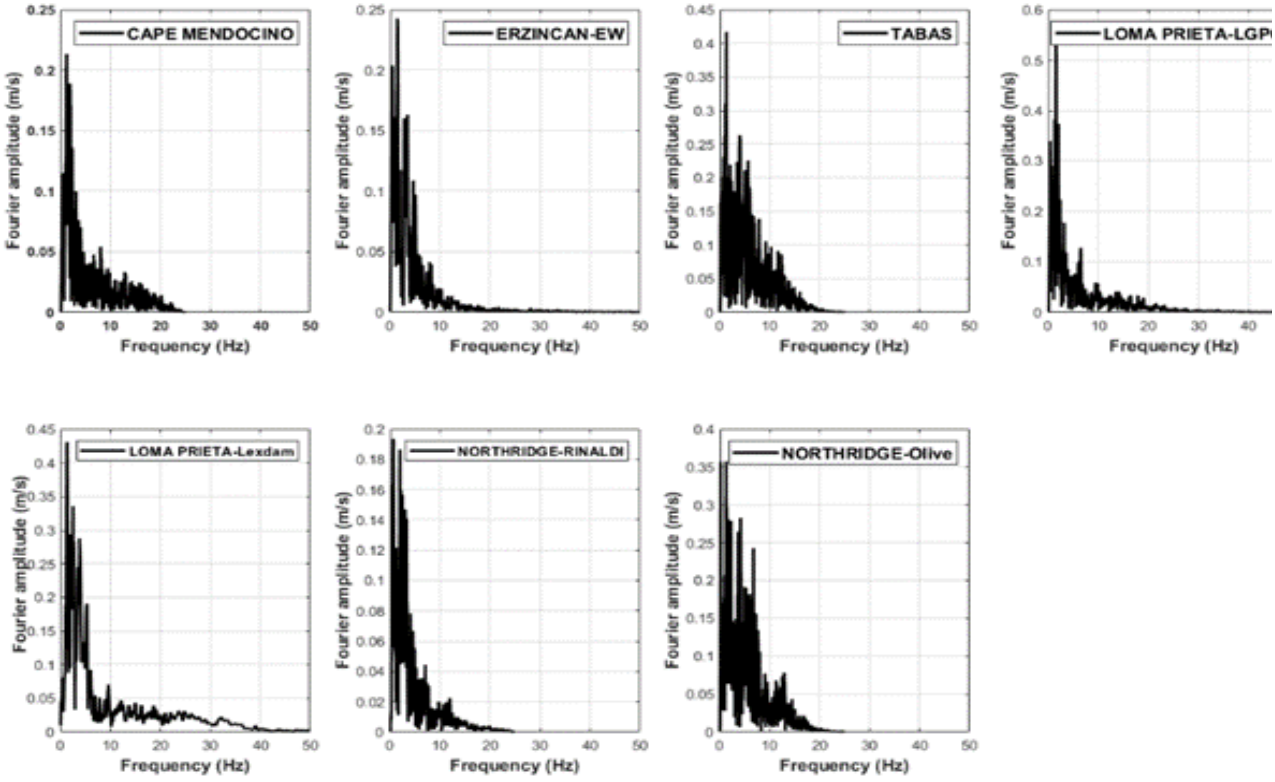

Figure 6. Fourier transform signals for the set of forward-directivity records.

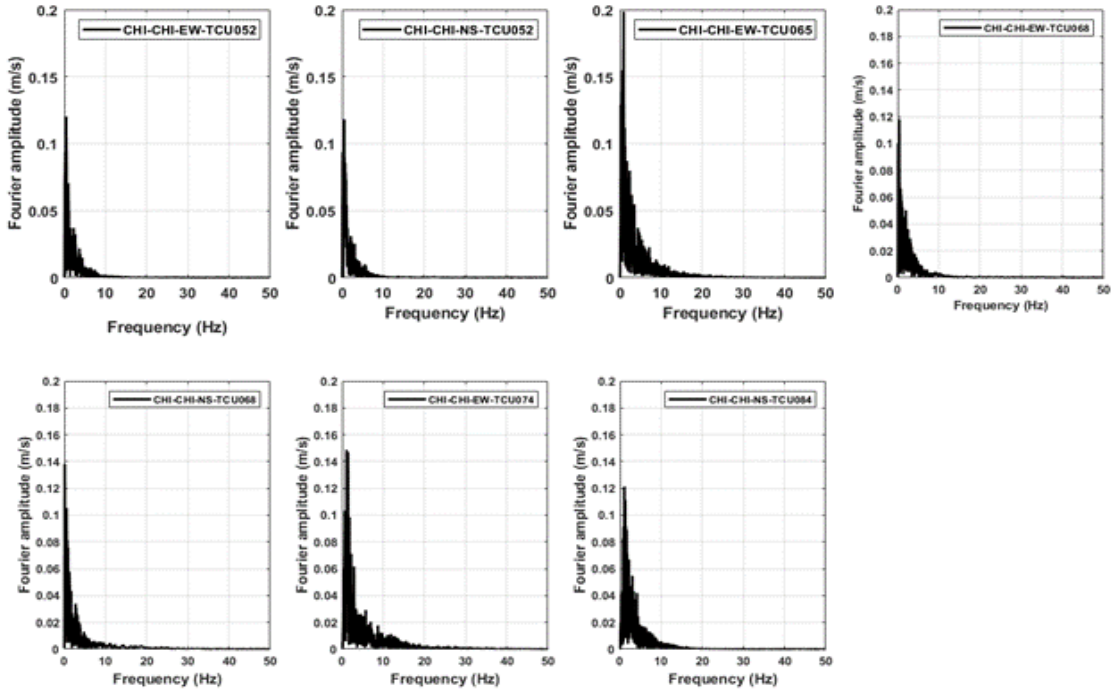

Figure 7. Fourier transform signals for the set of fling-step records.

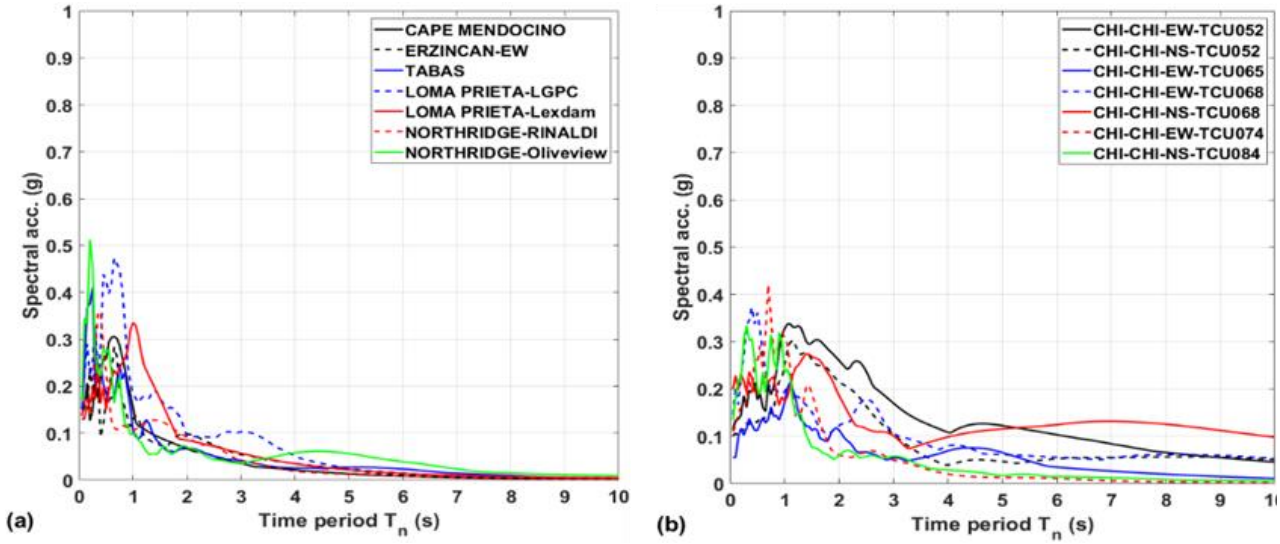

Figure 8. Acceleration response spectra at 5% critical damping for the set of (a) forward-directivity records, (b) fling-step records.

The current study uses Nonlinear Time History Analysis based on the Fast Nonlinear Analysis approach available in CSI-BRIDGE. The approach combines both modal superposition and nonlinear response calculations, allowing for efficient and accurate assessment of structural behavior under seismic excitation in addition, it approximates the nonlinear behavior of the structure by incorporating key nonlinear components such as the formation of plastic hinges in bridge piers while using modal response analysis based on the natural frequencies and mode shapes to capture the structural dynamic response. In particular, this approach is well-suited for structural engineering applications where a balance between computational efficiency and modeling accuracy is necessary. Given the complexity of near-fault ground motions with forward-

directivity and fling-step characteristics, this method enables the study to explore a wide range of structural responses efficiently, especially across varying pier heights.

5. Code limitations

5.1. International Building Code (IBC)

The main goal of a code-based design is to safeguard against major failures and loss of human life. International seismic codes such as the International Building Code (IBC) [33] place limitations on design and construction of structures in regions with different seismicity levels. The provided limitations are included in the code to ensure that the designed structures have the capability to resist seismic forces and reduce resulting damage and collapse. Key limitations include structural systems, structural irregularities, seismic design categories vary from (A-F) according to the expected earthquake and site class. Structures assigned to risk category "D through F" are given special requirements than those assigned to "A through C". Risk categories vary from (I-IV), specific structural requirements based on the structure's risk category are required. Risk category III and IV have lower allowable collapse probabilities than structures associated with risk category I and II. The code also defines drift and deflection limits based on the risk category to ensure structural integrity to prevent collapse and minimize expected damage during seismic events.

5.2. Egyptian Code (EC)

The Egyptian Code (EC) [29] for Loads provides comprehensive guidance on load limitations for various structures, including bridges and buildings. The specific outlined limitations by the code include load combinations for serviceability and ultimate limit states to ensure adequately designed structures to withstand the applied seismic loads. Design load factors to account for uncertainties and variations in loading conditions. The code also provides detailed procedures for calculating and distributing seismic loads accounting for influential factors such as supporting soil conditions, type of structure, and seismicity level as well. The ECP outlines the requirements for design verifications for structural elements under the calculated seismic loads.

6. Model Verification

To ensure the reliability and accuracy of the grillage model, a comparison has been conducted with the developed 3D Finite Element Models (FEM) of the hollow-core slab bridge. This comparison aimed to accurately capture the behavior of the deck slab elements, diaphragms, substructure and torsional effects. The grillage model predicted a deflection of 19.7 mm due to the total applied dead loads, as shown in Figure 1, while the 3D FEM model produced a deflection of 19.3 mm under the same applied loads (see Figure 2). The close percentage between the two models 97.9% demonstrates the accuracy of grillage method analysis and results.

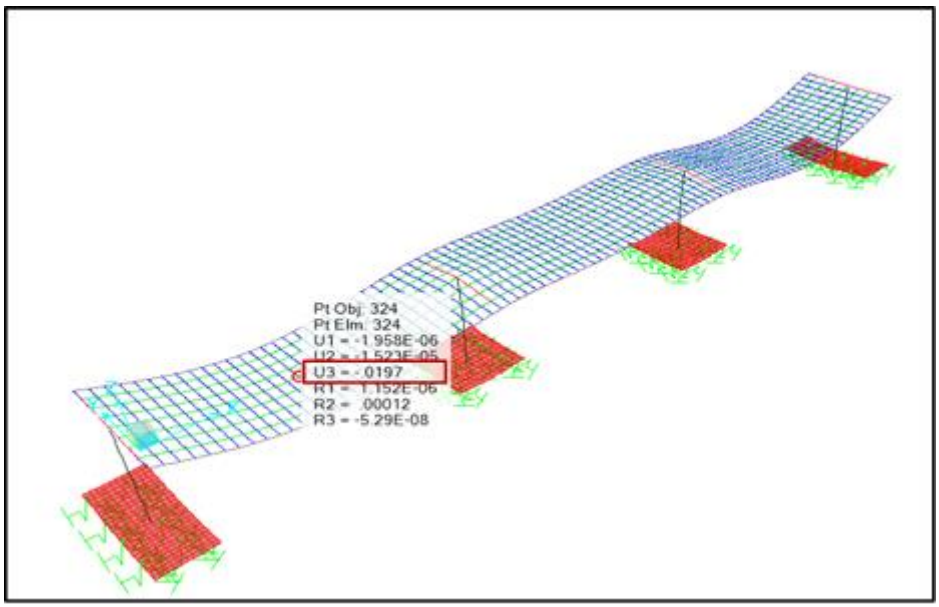

Figure 9. Grillage model of hollow core slab bridge.

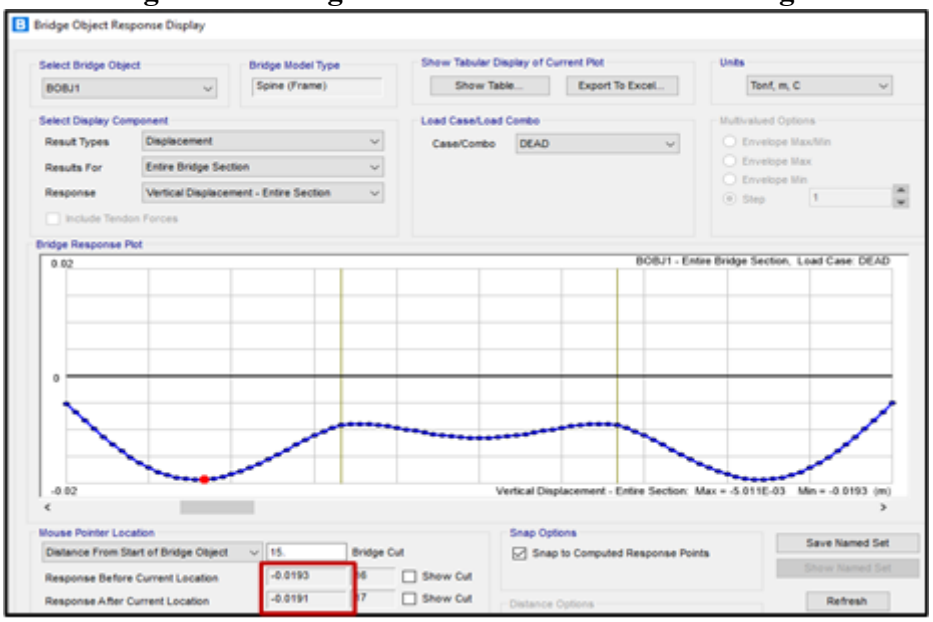

Figure 10. Developed 3D FEM model of hollow core slab bridge

7. Results and Discussions

7.1. Columns Displacement Response

Fig. 11 presents a comparative analysis of the horizontal displacement responses along the column height for various bridge models of column height varies from 12.0 m to 7.5 m through decreased interval of 1.5 m. The models were excited by the selected near-fault records with forward-directivity and fling-step. To enhance clarity and facilitate performance comparison, the figures are arranged in descending order of column's height.

Displacement responses generally reach their peak at the top of the column across all the analyzed bridge models and forcing earthquakes. The average peak displacements recorded at the column top under fling-step records are 102.16mm, 74.42mm, 63.40mm, and 47.17mm, for bridge models with column height varying from 12m, 10.5m, 9m, and 7.5m, respectively.

The corresponding values for under forward-directivity records are 64.96mm, 59.90mm, 49.60mm, and 40.16mm. From a percentage perspective, the mean displacement values indicate that fling-step records produce higher peak deflections than forward-directivity records by approximately 57%, 34%, 28%, and 17% for bridge models with 12m, 10.5m, 9m, and 7.5m columns, respectively. The overall results under the fling-step records induce significantly greater peak displacements than forward-directivity ones. The higher the column, the higher the influence of fling-step records on the induced peak column's displacement. However, with the decrease of column's height, the influence of fling-step records starts to decrease. From frequency content point of view, it can be observed from the presented results in Fig. 11 that Loma-Prieta earthquake with the lowest PGA/PGV ratio among the other forward-directivity records produces the largest deflection values, see Table 1 for all the considered bridge models. On the other hand, Tabas, the one with the highest PGA/PGV ratios produce the lowest deflection values. The EW and NS components of the Chi-Chi earthquake from stations TCU-052 and TCU-068 with lowest PGA/PGV ratios produce the largest deflection values compared with the other records particularly Chi-Chi records from station TCU-084 which has the largest PGA/PGV ratio and produces the lowest deflection values.

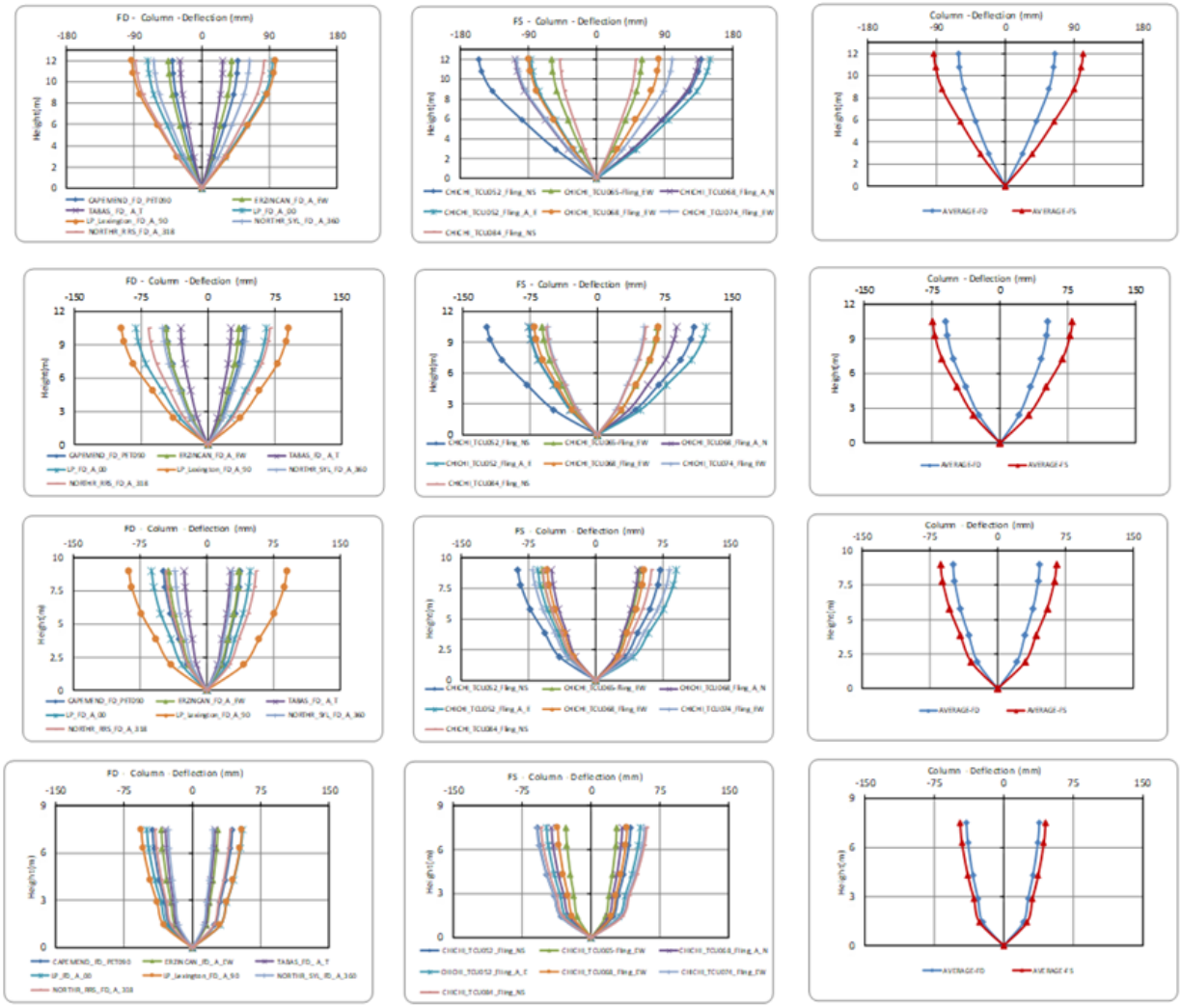

Figure 11. Column's peak displacements and average of peaks against column's height varying from 12.0 m to 7.5 m obtained under forward directivity and fling-step records

7.2. Columns Rotation Response

Fig. 12 illustrates the column's rotation response along its height for all considered bridge models subjected to forward-directivity and fling-step excitations. The column's rotation responses exhibit patterns similar to those observed in longitudinal displacement. However, the rotation response curves closely resemble a sinusoidal shape, with peak rotation occurring near the middle of the column height from the base. The average peak rotation values induced by fling-step events are 10.10 rad, 8.19 rad, 6.50 rad, and 4.49 rad for developed bridge models with column heights of 12.0 m, 10.5 m, 9.0 m, and 7.5 m respectively. The captured corresponding values under forward-directivity

Records are 6.55 rad, 5.45 rad, 5.16 rad, and 3.82 rad. These results indicate an increase in rotational demand due to fling-step records of approximately 53%, 50%, 26%, and 17.5% for models with column height of 12 m, 10.5 m, 9.0 m, and 7.5 m, respectively. The obtained results clearly indicate that fling-step records result in significantly greater peak rotation responses compared to forward-directivity records, with the effect of being more pronounced in the tallest columns. Regarding the frequency content, the obtained column's rotation results confirm that the higher the frequency content of the records, the lower the induced rotational response and vice-versa for both types of records.

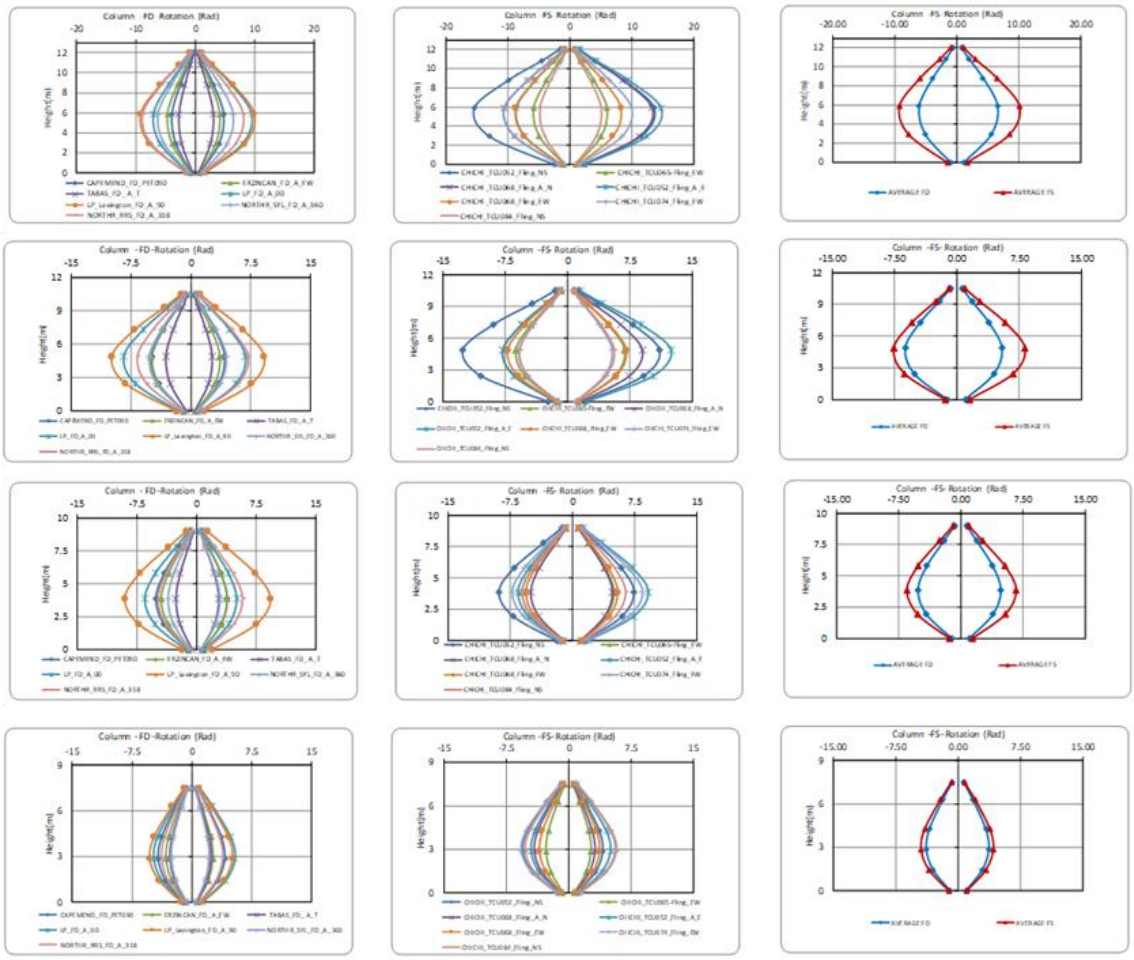

Figure 12. Column's peak rotation and average of peaks against column's height varying from 12 m to 7.5 m obtained under forward directivity and fling-step records.

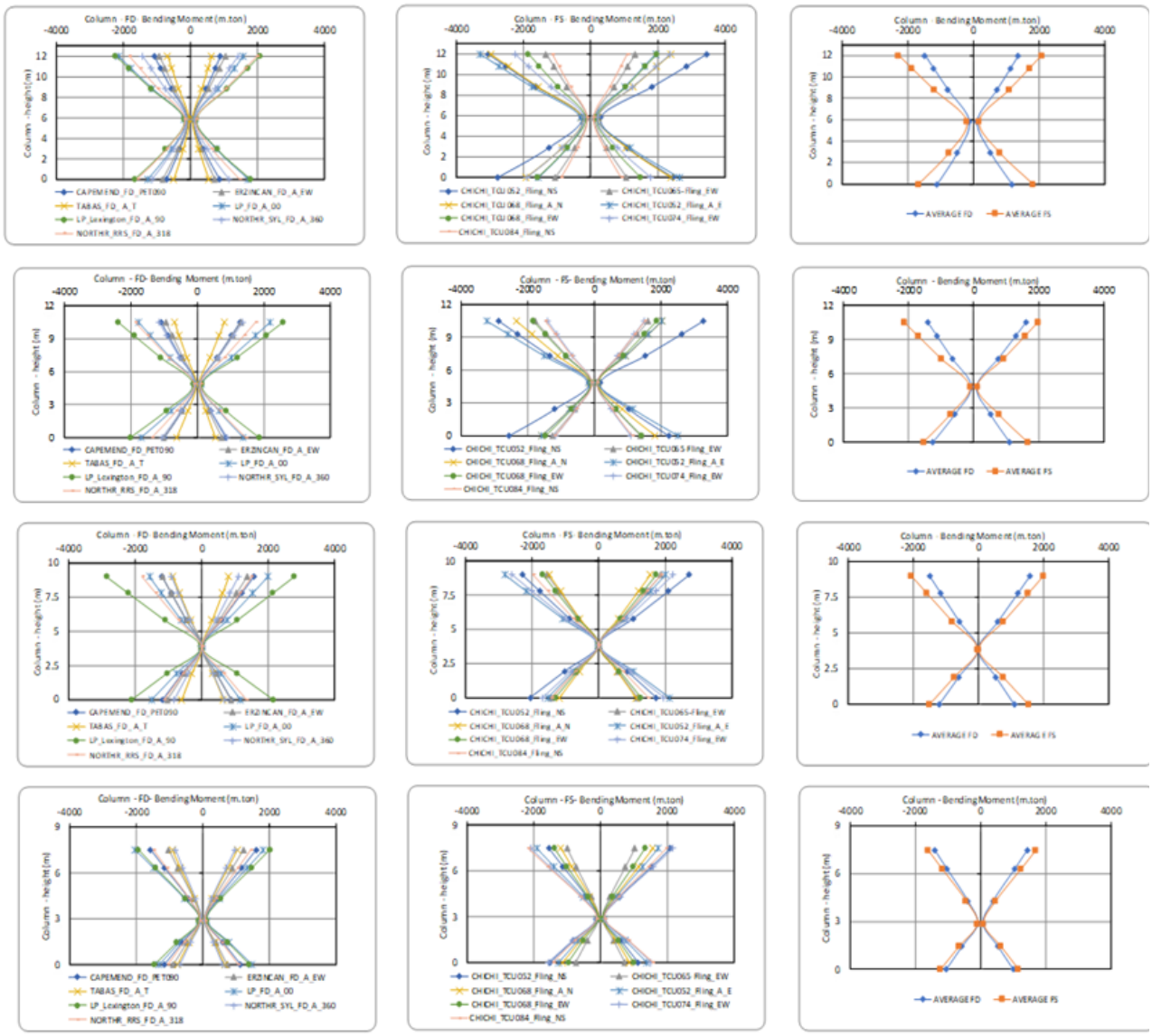

Figure 13. Column's peak bending moment and average of peaks against column's height varying from 12.0 m to 7.5 m obtained under forward directivity and fling-step records

7.3. Columns Bending Moment Response

Fig. 13 presents a comparative analysis of the column's bending moment responses along its height for various bridge models subjected to forward-directivity and fling-step excitations. As shown in the figure, the highest bending moment values occur at both ends of the column (i.e., at top and bottom of column), regardless of the type of applied loads and column height. Analysis of the moment distribution along the column's height reveals that the lowest moment values are concentrated near the middle of the column. The average peak bending moments recorded at the bottom of the column under fling-step records are 1820, 1660, 1505, and 1226 m.ton for bridge models with column's height of 12m, 10.5m, 9m, and 7.5m, respectively. The captured values, at the top of the column, are 2272, 2130, 1999, and 1699 m.ton. The corresponding values under the application of forward-directivity records, at the bottom are 1176, 1103, 1505, and 1042 m.ton, while at the top, they are 1476, 1416, 1589, and 1445 m.ton. From a percentage perspective, the mean values clearly indicate that fling-step records

produce higher average bending moments compared to forward-directivity records for all considered bridge models, with calculated values of almost 55%, 50%, 26%, and 18% for column heights of 12.0 m, 10.5m, 9.0 m, and 7.5 m, respectively. From frequency content point of view, the induced column's moment response is highly influenced by the ratio PGA/PGV. The lower the ratio, the higher the moment produced for the considered two types of records.

7.4. Columns Shear Force Response

A comparative analysis of the column shear force responses along the column's height for the considered different bridge models subjected to forward-directivity and fling-step excitations is presented in Fig. 14. Shear forces remain nearly constant along the column's height for all bridge models and earthquake records considered. The average peak shear force values recorded under fling-step events are 345, 339, 394, and 394 tons for models with column heights of 12.0 m, 10.5 m, 9.0 m, and 7.5 m, respectively. The corresponding values under forward-directivity records are 222, 275, 312, and 335 tons. These results show an increase in shear force demand of approximately 55%, 26%, 23%, and 18% for models with column heights of 12.0 m, 10.5 m, 9.0 m, and 7.5 m, respectively.

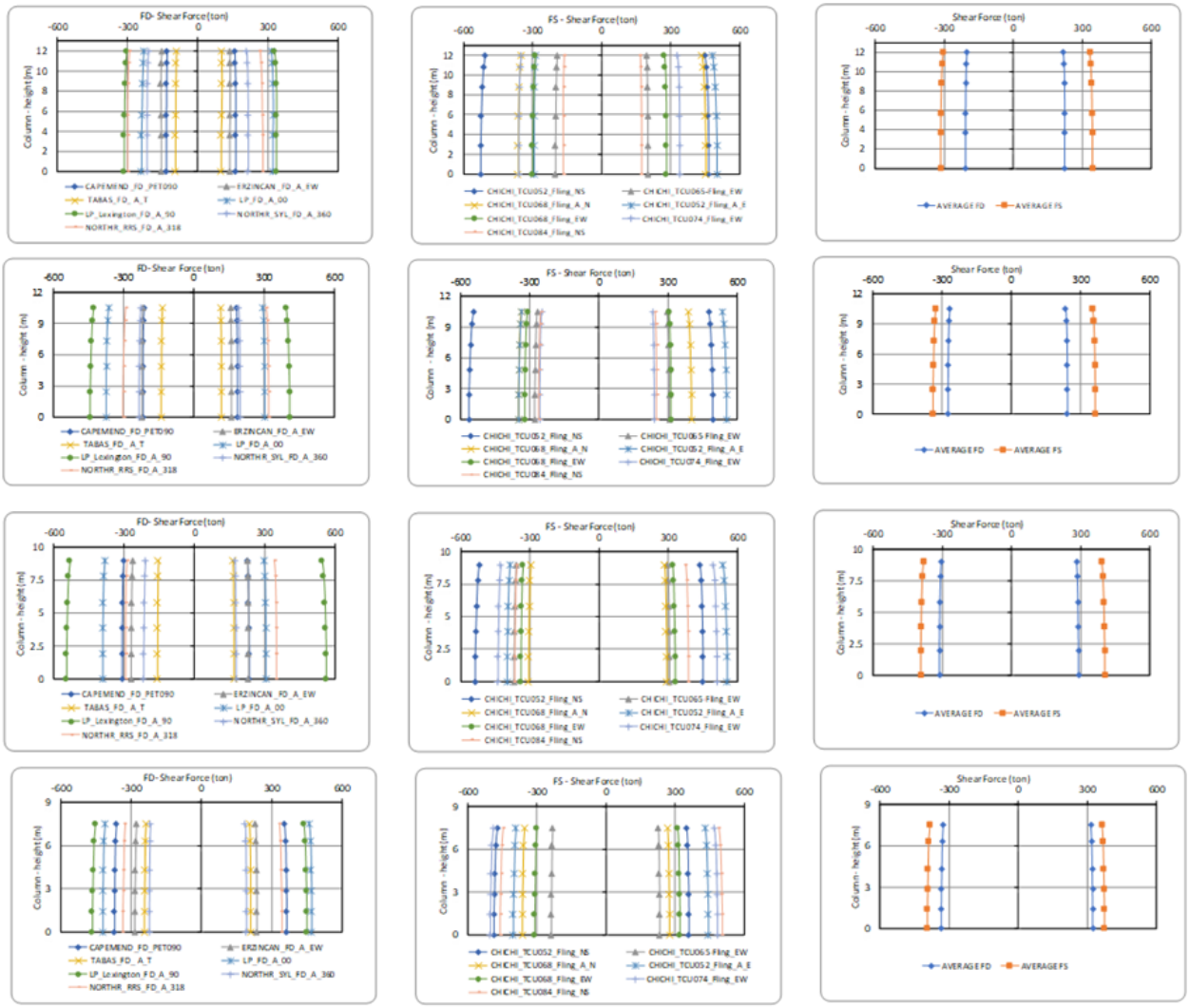

Fig. 14. Column's peak shear force and average of peaks against column's heights varying from 12.0 m to 7.5 m obtained under forward directivity and fling-step records.

8. Conclusions

This study investigates the effects of near-fault motions with forward-directivity and fling-step on the seismic response of columns of a hollow-core deck slab bridge with varying heights. Different bridge models with column heights ranging from 12.0 m to 7.5 m were developed and excited by the selected ground motion records representing forward-directivity and fling-step effects. All the developed models are of same span length and deck widths. The obtained results from the performed. Nonlinear time-history analysis reveals that columns' responses induced by forward-directivity records significantly differ from those by fling-step records. The average peaks of column's straining actions are consistently higher for fling-step records for the considered bridge models. The effect is highly pronounced for bridge models with the highest columns and reduces as the column's height decreases. The frequency content ratio, i.e., PGV/PGA ratio, has been found to influence the induced column's responses, where records with low ratio of PGA/PGV produce high deflection response values and vice-versa.

References

[1] Yadav KK, Gupta VK. Near-fault fling-step ground motions: characteristics and simulation. Soil Dyn Earthq Eng, 2017;101:90–104. https://doi.org/10.1016/j.soildyn.2017.06.022

[2] Zhang, F.; Li, S.; Wang, J.; Zhang, J. Effects of fault rupture on seismic responses of fault-crossing simply-supported highway bridges. Eng. Struct. 2020, 206, 110104.

[3] Luo, Q.; Dai, F.; Liu, Y.; Chen, X. Simulating the near-field pulse-like ground motions of the Imperial Valley, California, earthquake. Soil Dyn. Earthq. Eng. 2020, 138, 106347.

[4] Yang, S.; Mavroeidis, G.P.; Ucak, A. Analysis of bridge structures crossing strike-slip fault rupture zones: A simple method for generating across-fault seismic ground motions. Earthq. Eng. Struct. Dyn. 2020, 49, 1281–1307

[5] Dong, Z.; Sun, Z.; Wu, S.; Tong, F.; Wang, D. Influence of soil liquefaction effect on seismic failure mechanism of river-crossing simply-supported girder bridges subjected to near-fault ground motions. Engi. Fail. Anal. 2023, 154, 107664.

[6] Bray JD, Rodriguez-Marek A. Characterization of forward-directivity ground motions in the near-fault region. Soil Dyn Earthquake Eng 2004;24(11):815–828. http://dx.doi.org/10.1016/j.soildyn.2004.05.001

[7] Makris N, Black CJ. Evaluation of peak ground velocity as a "good" intensity measure for near-source ground motions. J Eng Mech 2004;130(9):1032–1044. https://doi.org/10.1061/(ASCE)0733-9399(2004)130:9(1032)

[8] Adanur, S., Altunişik, A.C., Bayraktar, A. et al. Comparison of near-fault and far-fault ground motion effects on geometrically nonlinear earthquake behavior of suspension bridges. Nat Hazards 64, 593–614 (2012). https://doi.org/10.1007/s11069-012-0259-5

[9] Gorai S, Maity D. Seismic response of concrete gravity dams under near field and far field ground motions. Eng Struct 2019; 196: 109292. https://doi.org/10.1016/j.engstruct.2019.109292

[10] Park SW, Ghasemi H, Shen J, et al. Simulation of the seismic performance of the Bolu Viaduct subjected to near-fault ground motions. Earthquake Eng Struct Dyn 2004;33(13):1249–1270. https://doi.org/10.1002/eqe.395

[11] Shen J, Tsai MH, Chang KC, Lee GC. Performance of a seismically isolated bridge under near-fault earthquake ground motions. J Struct Eng 2004;130(6):861–8. https://doi.org/10.1061/(ASCE)0733-9445(2004)130:6(861)

[12] Wang J, Zou X, Yan X, et al. Integrated analysis model for the seismic responses of cable-stayed bridges near active faults. J Earthquake Tsunami 2015;9(01):1550002. http://dx.doi.org/10.1142/S1793431115500025

[13] Pan Y, Shi S, Chang Z, Hu S. Quantitative study on amplification effect of base isolated structures subjected to near-fault pulse-like ground motions. China Civil Eng J 2018;51(11):8–16.

[14] Ma H, Zhuo W, Gu Y. Displacement response analysis of regular highway girder bridges under near-fault

pulse-type ground motions. China J Highway Transport 2017;30(12):139–149.
[15]. Jin, S.; Wang, D.; Jiang, D. Seismic fragility analysis of containment structure subjected to near fault ground motions. Prog. Nucl. Energy 2023, 161, 104734. [CrossRef]
[16]. Kawashima, K. Damage of bridges resulting from fault rupture in the 1999 Kocaeli and Duzce, Turkey earthquakes and the 1999 Chi-Chi, Taiwan earthquake. Struct. Eng. Earthq. Eng. 2002, 19, 179s–197s.
[17]. Zhong, J.; Jiang, L.; Pang, Y.; Yuan, W. Near-fault seismic risk assessment of simply supported bridges. Earthq. Spectra 2020, 36, 1645–1669
[18]. Goel, R.K.; Chopra, A.K. Analysis of ordinary bridges crossing fault-rupture zones. In Proceedings of the 14th World Conference on Earthquake Engineering, Rep. No. UCB/EERC-2008, Beijing, China, 12–17 October 2008; Volume 1.
[19]. Yang, S.; Mavroeidis, G.P. Bridges crossing fault rupture zones: A review. Soil Dyn. Earthq. Eng. 2018, 113, 545–571.
[20] Kawashima K. Damage of bridges resulting from fault rupture in the 1999 Kocaeli and Duzce, Turkey earthquakes and the 1999 Chi-Chi, Taiwan earthquake. Struct Eng/Earthquake Eng 2002;19(2):179.
[21] Li J, Xu LH. Seismic response characteristics and whiplash effect mechanism of continuous rigid-frame bridges subjected to near-fault ground motions. Bull Earthq Eng 2023; 21: 3719-3744. https://doi.org/10.1007/s10518-023-01672-4
[22] Zheng SX, Shi XH, Jia HY, Zhao CH, Qu HL, Shi XL. Seismic response analysis of long-span and asymmetrical suspension bridges subjected to near-fault ground motion. Eng Fail Anal 2020; 115: 104615. https://doi.org/10.1016/j.engfailanal.2020.104615
[23] Xin L, Li X, Zhang Z, Zhao L (2019) Seismic behavior of long-span concrete-flled steel tubular arch bridge subjected to near-fault fing-step motions. Eng Struct 180:148–159. https://doi.org/10.1016/j.engstruct.2018.11.006
[24] Alothman A, Mangalathu S, Al-Mosawe A, Alam MD, Allawi A. The influence of earthquake characteristics on the seismic performance of reinforced concrete buildings in Australia with varying heights. Journal of Building Engineering, 2023; 67: 1-16. https://doi.org/10.1016/j.jobe.2023.105957
[25] Alothman A, Mangalathu S, Hashemi J, Al-Mosawe A, Alam MD, Allawi A. The effect of ground motion characteristics on the fragility analysis of reinforced concrete frame buildings in Australia. Structures, 2021; 34: 3583-3595. https://doi.org/10.1016/j.istruc.2021.09.084
[26] Srivastava C, Pandikkadavath MS, Mangalathu S, AlHamaydeh M. Seismic response of RC bridges under near-fault ground motions: A parametric investigation. 2024; 61. https://doi.org/10.1016/j.istruc.2024.106033
[27] Nanclares G, Curadelli O, Ambrosini D. Influence of the vertical seismic component on the response of continuous RC bridges. 2024; 305. https://doi.org/10.1016/j.compstruc.2024.107558
[28] Wei W, Shao C, Wang C, Zhuang, W. Seismic performance of near-fault girder bridges based on laminated rubber bearings under the impact of sequential earthquakes. 2024. https://doi.org/10.1080/15732479.2024.2423039
[29] ECP (2012) - ECP-201, "Egyptian code for calculating loads and forces in structural work and masonry", Housing and Building National Research Centre. Ministry of Housing, Utilities and Urban Planning, Cairo, 2012.
[30] Kianoush, M. R. and Ghaemmaghami, A.R. (2011).The effect of earthquake frequency content on the seismic behavior of concrete rectangular liquid tanks using the finite element method incorporating soil–structure interaction, Engineering Structures. v. 33 pp 2186–2200. https://doi.org/10.1016/j.engstruct.2011.03.009
[31] Kalkan E, Kunnath SK (2006) Effects of fling step and forward directivity on seismic response of buildings. Earthq. spectra 22:367–390. https://doi.org/10.1193/1.2192560.
[32] Mahmoud S, Alqarni A, Saliba J, Ibrahim AH, Diab H (2021) Influence of floor system on seismic behavior of RC buildings to forward directivity and fling-step in the near-fault region. Structures 2021; 30:2 803-817. https://doi.org/10.1016/j.istruc.2021.01.052
[33] IBC 2021: International Building Code. ICC Publications, 2020.